JTTEE5 9:90-94

Microstructure of a Plasma-Sprayed Mo-Si-B Alloy

M.J. Kramer, S.C. Okumus, M.F. Besser, Ö. Ünal, and M. Akinc

(Submitted 9 February 1999; in revised form 7 December 1999)

Powders of $Mo_{52}Si_{38}B_{10}$ were plasma sprayed under inert conditions onto stainless steel substrates to determine if high density free standing forms could be synthesized by this process. Thermal spray conditions were varied to minimize porosity and oxygen impurities while minimizing evaporative metal losses. The as-sprayed and sintered microstructures were characterized using scanning and transmission electron microscopy and quantitative x-ray diffraction (XRD). The as-sprayed microstructure consisted of elongated splats tens of microns in length and only one to three microns in thickness. The splats contained submicrometer grains of primarily MoB and $Mo_5Si_3B_x$ (T1) and minor amounts of $MoSi_2$ and a glassy grain boundary phase. The interior of the splats typically consisted of a fine eutectic of MoB and T1.

Small pieces were cut out of the cross section of the sample and pressureless sintered for 2, 6, and 10 h at 1800 °C in flowing Ar. After sintering for 2 h at 1800 °C, the samples exhibited a coarser but equiaxed microstructure (1 to 5 μm grain size) containing 78 vol.% T1, 16 vol.% MoB, and 6 vol.% $MoSi_2$ as determined by XRD. Approximately 8 at.% of the Si formed silica. The high-temperature anneal removed all vestiges of the layered structure observed in the as-sprayed samples.

Keywords silicide, evaporation, $Mo_5Si_3B_x$, $MoSi_2$, XRD, TEM

1. Introduction

Producing fine-grained and dense alloys out of refractory intermetallics is a technically difficult task. The high temperatures involved with melting and subsequent slow cooling of castings lead to excessive grain growth, especially in the silicides.[1] Large grains typically result in numerous microcracks due to highly anisotropic coefficients of thermal expansion. Powder processing is an alternative route to fabricating a fine-grained homogeneous sample, but the high temperatures necessary for sintering make producing dense samples difficult.[2,3] In addition, surface contamination from C or O is problematic with the silicides since C stabilizes the hexagonal polymorph of the Mo_5Si_3 and O leads to the formation of silica, which can have a detrimental effect on their strength.[4,5]

Thermal spraying has been demonstrated as a viable technique to producing fine-grained, homogeneous samples from complex intermetallics.[6,7] The small size of the individual splats (tens of microns) and their relatively rapid cooling reduce the spatial scale of the solidifying phases (<1 μm). However, chemical homogeneity and morphology of the starting powders strongly influence the chemical and physical properties of thermal-sprayed coatings.[8] The finer the spatial scale of the chemical inhomogeneities and the more spherical the powder morphology, the better the overall coating properties.[9] Air plasma spraying (APS) yields highly metastable microstructures in both films and free-standing forms.[10] Thermal spraying in a chamber below atmospheric pressure or low pressure plasma spraying (LPPS) is an alternative method to produce dense deposits with enhanced interparticle bonding.[11,12]

M.J. Kramer, S.C. Okumus, M.F. Besser, Ö. Ünal, and **M. Akinc,** Ames Laboratory, Iowa State University, Ames, IA 50011.

In this paper, the effect of varying thermal spraying parameters on the formation of the microstructure in a Mo-Si-B system is discussed. Spraying conditions were varied to minimize the elemental losses and contamination of C, N, and O. Once the thermal spraying parameters were optimized, large monoliths ($90 \times 90 \times 10$ mm) were fabricated. Parts of the monoliths were subsequently sintered at 1800 °C for 2 to 10 h to densify and remove inhomogeneities inherent in the thermal-sprayed process. The mechanical properties and oxidation resistance of these samples were reported elsewhere.[3,5]

2. Experimental Techniques

2.1 Characterization

Chemical and phase analyses of the starting powders and the coatings were performed using a number of techniques. Bulk chemical analysis was performed using a Thermal Jarrel-IRIS Advantage (Jarrel ICP-AES, Franklin, MA) inductively coupled plasma-atomic emission spectrograph (ICP-AES) system on samples digested in a 2:2:1 solution of HCl, HNO_3, and HF without heating. Light elements were determined by inert gas fusion (IGF). Nitrogen and oxygen were measured using a LECO TC-436 (LECO Corporation, St. Joseph, MI) and carbon with a Horiba (Horiba, Kyoto, Japan) EMIA 520. The error for the ICP-AES is 3% relative and that for IGF is 1%. Phase analysis was performed using powder X-ray diffraction (XRD) with Cu_α. The XRD was performed on either a Scintag (Scintag, Cupertino, CA) X1 with a solid-state detector or a Philips (Philips Electronic Instruments Corp., Mahwah, NJ) 1870 with a scintillator detector. Electron microscopy was performed using a JEOL 6100 (Japan Electron Optics Ltd., Tokyo) or Amray (Amray, Bedford, MA) 1840 SEM and a Philips CM30 TEM. Cross-sectional morphologies were examined in the SEM to determine the size and homogeneity of the phases in individual splats. Given the fine grain size of the as-sprayed morphology, the TEM was used to analyze the phase

assemblages and the sequence of solidification in the optimally sprayed samples. Electron diffraction was used to distinguish between crystalline and amorphous phases, while elemental analysis was performed by energy dispersive spectroscopy (EDS) or electron energy loss spectroscopy (EELS).

2.2 Starting Powder

A large batch (~20 kg) of Mo-Si-B powder was obtained from a commercial vendor (Exotherm Inc., Camden, NJ). The powder particles were nominally spherical (Fig. 1) and therefore ideal for thermal spraying. The powder was sized using standard sieves to three size fractions: <45 μm, 45 to 75 μm, and >75 μm. Aliquots of the as-received powder and the two smaller size fractions were analyzed using ICP-AES for Mo, Si, and B and IGF for C, N, and O elemental analysis (Table 1). Note the variation in elemental composition between the various size fractions, which is statistically significant for the major elements, indicating a chemical inhomogeneity across these classifications. Although qualitative, energy dispersive spectroscopy (EDS) of the powders in the SEM indicated that there are chemical variations from particle to particle within the 45 to 75 μm size used in this study. In addition, O and C impurities are quite high. The implications of large concentrations of impurities will be discussed later.

3. Thermal Spraying

Thermal spraying was performed using Miller Thermal SG-100 plasma spraying equipment (Miller Thermal, Inc., Appleton, WI). Due to the volatility of Si, and susceptibility of Mo to oxidation, an initial screening study was performed to determine the optimal thermal spraying parameters. The adjustable parameters included the spraying chamber atmosphere, substrate materials, stand-off distance from the nozzle, and thermal spray parameters: current (900 to 950 amps), voltage (43 to 53 V), and gas flow rates. In air spraying, the Ar powder gas was set to 0.3 MPa (40 psi), while for Ar atmosphere spraying, the powder gas was set to 0.6 MPa (85 psi). The Ar arc gas was held at 0.5 MPa (65 psi). The auxiliary He gas was varied from 1.0 to 1.1 MPa (150 to 165 psi).

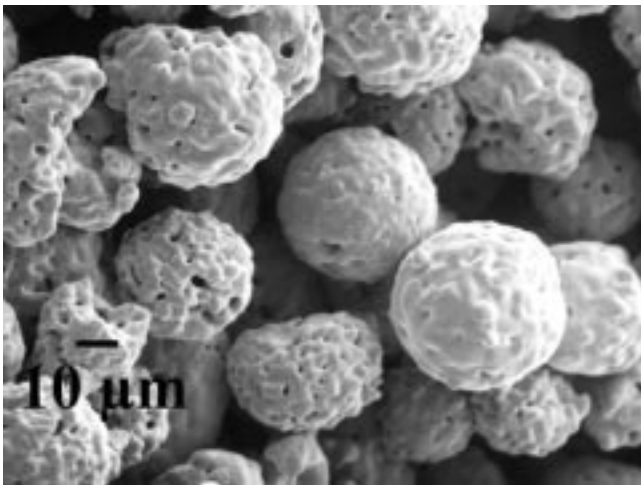

Fig. 1 SEM micrograph of the as-received powder. Note that the spherical particles are porous aggregates of smaller (~1 to 3 μm) crystallites.

3.1 Spraying in Air

Substrates of mild steel were degreased in an aqueous degreaser for 15 min. The steel was rinsed in water and ethanol and then dried. The surface was roughened by high pressure 24 grit Al_2O_3 and ultrasonically cleaned in ethanol. Four stand-off distances were tested by spraying deposits of approximately 300 μm in thickness using multiple passes. Chemical analysis showed that Si loss increased with increasing stand-off distance and that O content increased by a factor of 3 to 4 compared to the starting composition (Table 2). The high Si loss and large increase in O indicated that thermal spraying had to be performed in an inert environment to maintain initial chemical composition. Carbon was not analyzed since it was a minor constituent (Table 1).

3.2 Spraying in Argon

Thermal spraying in a sealed chamber filled with Ar with a reduced pressure (300 torr) resulted in samples closer to the initial chemical composition than when using the spray conditions discussed above (Table 3). The Mo:Si ratio was slightly higher than initially measured, but the increase of oxygen was less than in air. Within the error of the analysis, there was no difference in overall chemical composition with stand-off distances from 10.2 to 22.9 cm (4 to 9 in.) in contrast to air spraying, which showed increasing Si losses with the increasing spray distance. A stand-off

Table 1 ICP analysis for the as-received powders and after sieving

At.%	As-received powder	As-received powder −75 + 45 μm	As-received powder −45 μm
Mo	52.7	51.1	48.3
Si	35.7	37.2	37.4
B	9.2	10.1	12.4
O	2.43	1.24	1.40
N	0.05	0.02	0.04
C	. . .	0.23	0.51

Table 2 ICP analysis of as-sprayed samples in air for various stand-off distances

	Stand-off distances			
At.%	3 in. 7.62 cm	5 in. 12.70 cm	7 in. 17.78 cm	9 in. 22.86 cm
Mo	55.1	57.8	60.2	62.3
Si	31.0	29.0	26.4	23.6
B	9.3	9.4	9.7	9.2
O	4.41	3.66	3.56	4.59
N	0.20	0.19	0.20	0.26

Table 3 ICP analysis of as-sprayed samples in Ar for various stand-off distances

	Stand-off distances			
At.%	4 in. 10.16 cm	6 in. 15.25 cm	8 in. 20.32 cm	9 in. 22.86 cm
Mo	52.8	52.7	52.9	52.9
Si	35.3	35.7	35.6	35.3
B	9.0	8.7	8.9	9.0
O	2.82	2.84	2.55	2.76
N	0.08	0.07	0.05	0.06

of 13 cm (5 in.) was used as a compromise between excessive heating of the substrate during deposition and radiant cooling between passes when building up thick samples (>1 mm).

Optimization of Spraying Parameters. The current, voltage, and auxiliary gas pressure were varied to optimize the spraying parameters with the 13 cm (5 in.) stand-off distance (Table 4). The higher parameters showed the least deviation from initial composition, in particular, the lowest oxygen gain. The low oxygen content is of special importance, since larger mass fraction of oxygen would indicate a potential to form a large fraction of silica, which in turn could be detrimental to the mechanical properties. These optimized parameters were then used in preparing smaller, but thicker (5 versus 0.3 mm) samples.

Substrate Determination. The small bulk coating pretrials included testing of substrate types (6.35 mm graphite, 12.7 mm stainless steel, and 9.53 mm Mo) and the surface preparation. In the following table, NGB signifies no grit blasting, LGB light grit blasting, and GB normal grit blasting. Since the goal is to fabricate free-standing monolithic samples suitable for mechanical testing, a substrate with poor adhesion qualities was desired. Using the optimized parameters listed in Table 4, coatings of nominally 5 mm in thickness were fabricated. Samples on stainless steel showed the least adhesion to the substrate. Samples on stainless steel substrates also exhibited the lowest impurities of C, N, and O, but the effect was small. High carbon values, from the graphite substrate, may result in formation of the hexagonal structure, while an oxide coating on the Mo could have contributed the higher oxygen values. The Mo was a particularly poor choice for a substrate since the adhesion was very strong and the tile could not be removed.

Three tiles ($90 \times 90 \times 10$ mm) suitable for mechanical testing were then produced on stainless steel using these same parameters (Table 5).[5] The microstructures of these larger pieces were then studied in depth. Parts of these larger tiles were also heat treated in Ar up to 1800 °C for up to 10 h to determine the effect of annealing on grain size and phase changes.

4. Microstructural Analysis

The crystalline phase assemblages were studied by performing full pattern Rietveld refinements. This allowed for quantitative determination of the volume fraction of the crystalline phases. Both an SEM and a TEM were employed to analyze the microstructure. The grain size of the as-sprayed materials was too fine (generally submicrometer) to resolve adequately in the SEM. However, the SEM was helpful in observing the larger scale inhomogeneities, particularly in backscattered electron images.

4.1 As-Sprayed Microstructure

The as-sprayed material showed a layered-like structure perpendicular to the spraying direction (Fig. 2). The individual splats were elongated (up to 10 μm by 1 to 3 μm thick) yet irregular in shape. Both inter- and intrasplat fracturing were observed. The measured density was 7.41 g/cm^3 (or ~90% theoretical). The XRD results showed that the crystalline phases were predominately $Mo_5Si_3B_x$ (T1), MoB, and a small amount of $MoSi_2$. In addition to these phases, a TEM micrograph of the cross section revealed both silica and a metallic glass of Mo-Si-B. The qualitative composition of the metallic glass (met-glass) was determined by EDS and EELS, while the glassy nature was demonstrated using microdiffraction. The boundaries between the splats was easily identified and was always composed of amorphous material, predominately the met-glass, which contained Mo-Si-B but no oxygen as determined by EELS. Silica was observed, but formed as spherical particles within the interior of the splats and not at the splat boundaries. Although the thinning process for transmission electron microscopy results in a near two-dimensional sampling, it was clear that the phase proportions and the grain sizes within individual and between neighboring splats varied considerably. Some splats were almost entirely T1, while others had high proportions of MoB and $MoSi_2$.

The TEM also revealed a distinct solidification sequence for the individual splats. The boundary between the splats was a thin amorphous layer (50 nm), which gives way to a thicker nanophased region (up to a few hundreds of nanometers thick) (Fig. 3) and then a eutectic microstructure, typically of MoB and T1, as shown in Fig. 4. Dark-field imaging using the $\mathbf{g}_{200}$ reflection of the MoB shows that the cells of MoB all have the same orientation, indicating that MoB is the primary solidifying phase

Table 4 Effect of spraying parameters on composition

At.%	900 A 43 V 150 psi	950 A 52 V 165 psi
Mo	53.1	53.8
Si	33.7	33.7
B	10.3	10.4
O	2.78	2.07
N	0.11	0.06

Table 5 Composition of large ($90 \times 90 \times 10$ mm) tiles

At.%	Tile 1	Tile 2	Tile 3
Mo	52.2	52.7	53.0
Si	33.3	33.3	33.6
B	10.7	10.5	10.5
O	2.77	0.20	0.24
N	0.15	0.13	0.16
C	0.83	3.14	2.45

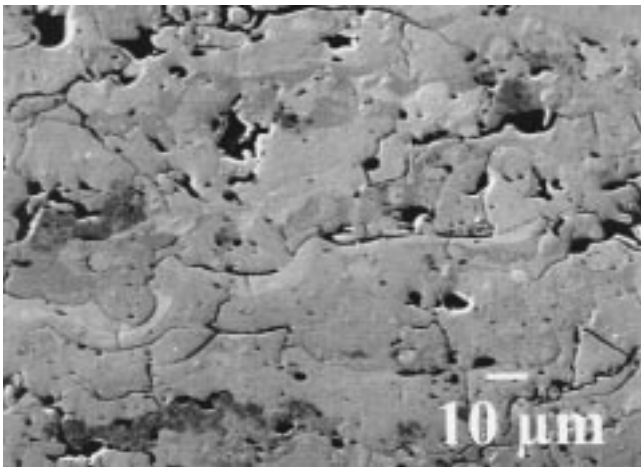

Fig. 2 SEM micrograph of the as-sprayed microstructure in an inert atmosphere. The spray direction is from the top to bottom in this micrograph.

(Fig. 4b), as expected since its melting temperature (2600 °C) is considerably higher than T1 (2180 °C). The cell size of the MoB varies considerably from splat to splat, indicating that the driving force (*i.e.*, the amount of undercooling) or that the composition changes from splat to splat. This is not unexpected, since the starting powder was suspected to be inhomogeneous.

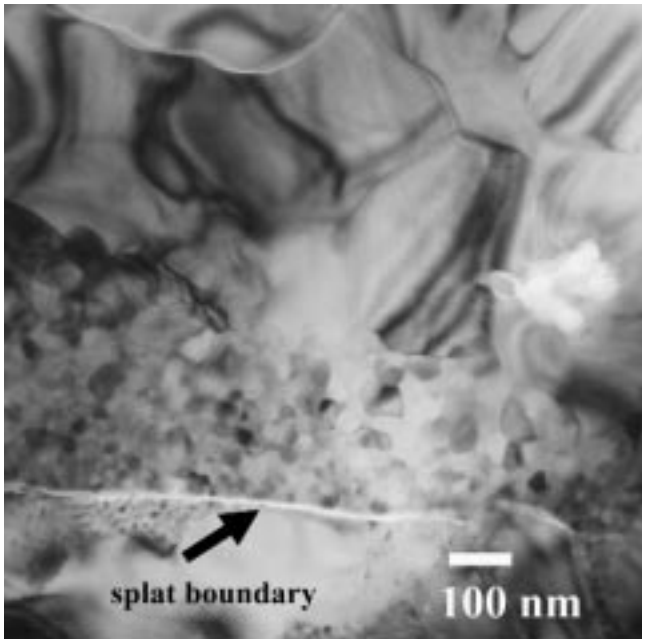

Fig. 3 TEM micrograph of the splat boundary showing the rapid transition from amorphous to nanocrystalline to coarsely crystalline microstructure. The nanophased region is a mixture of T1 and MoB.

Near the top half of the splats, the grain size has coarsened to about 0.5 to 1 μm and was typically T1 with an intergranular phase of $MoSi_2$. Nearly spherical inclusions (up to 0.5 μm) of silica were observed within some individual splats (Fig. 5). This large variation in chemical composition on such a fine spatial scale, as well as a fine to amorphous grain size, indicates a large driving force for recrystallization during annealing.

4.2 Annealed Microstructure

Parts of the larger tiles were heat treated in Ar at 1800 °C for 2, 6, and 10 h (Table 6). This resulted in complete recrystallization of the as-sprayed microstructure (Fig. 6). Density measurements for 2, 6, and 10 h were 7.61 g/cm^3 (~93% of theoretical), 7.68 g/cm^3 (~93.3%), and 7.77 g/cm^3 (~95%), respectively. The $MoSi_2$ appears to aggregate into larger regions instead of being uniformly dispersed through the sample. This may be a result of the initial inhomogenity. The MoB is well dispersed and usually finer in size (5.76 μm) than T1 (11.65 μm). Pockets of silica near triple points were identified by EDS in the SEM and TEM. Given the high oxygen content and the clear indication of silica in the SEM and by optical microscopy, it is estimated that approximately 8 wt.% of the sample is silica. The low strength and high ductility of four-point bend specimens at 1200 °C were attributed to this high silica content.[5]

5. Conclusions

Thermal spraying has been demonstrated as a viable means to produce dense monolithic samples of an alloy of Mo-Si-B. The critical parameters to maintain the starting stoichiometry are identified. This included thermal spraying in an inert environment to minimize the oxidation of the metal constituents and

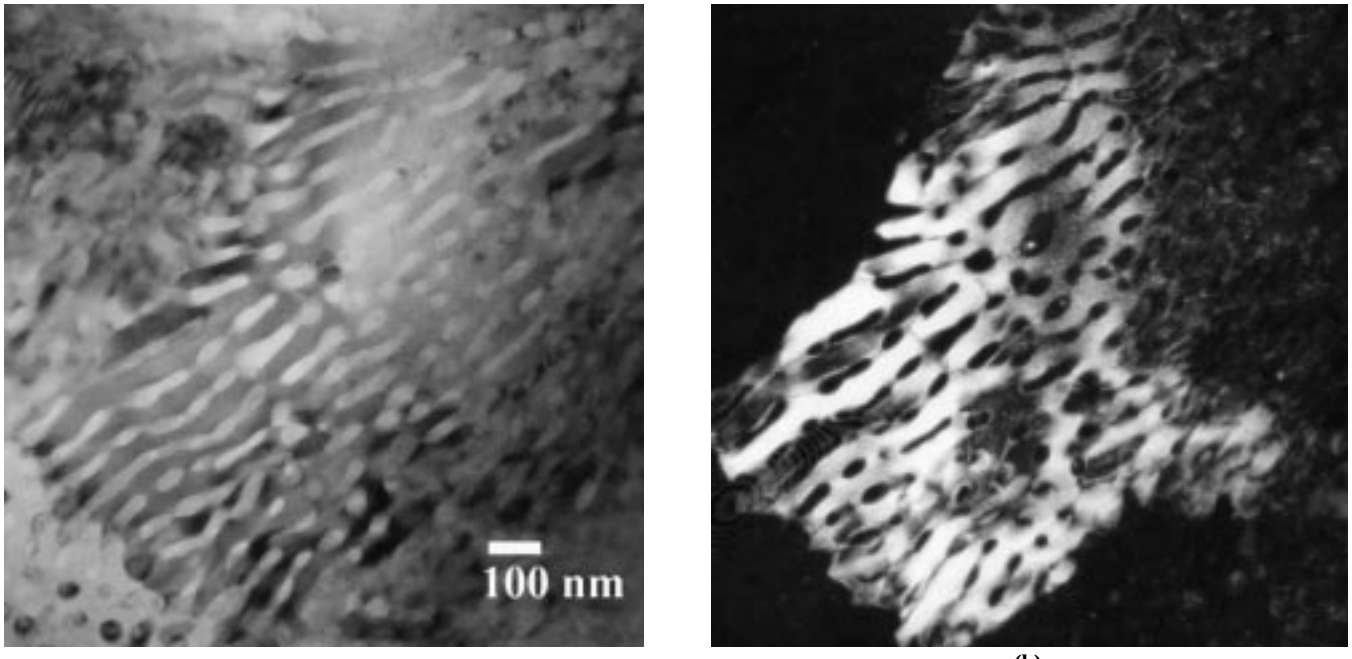

(a) **(b)**

Fig. 4 TEM micrograph of a coupled growth region showing a eutectic microstructure of MoB and T1.**(a)** Bright-field image and**(b)** dark-field image showing the columnar growth of the MOB

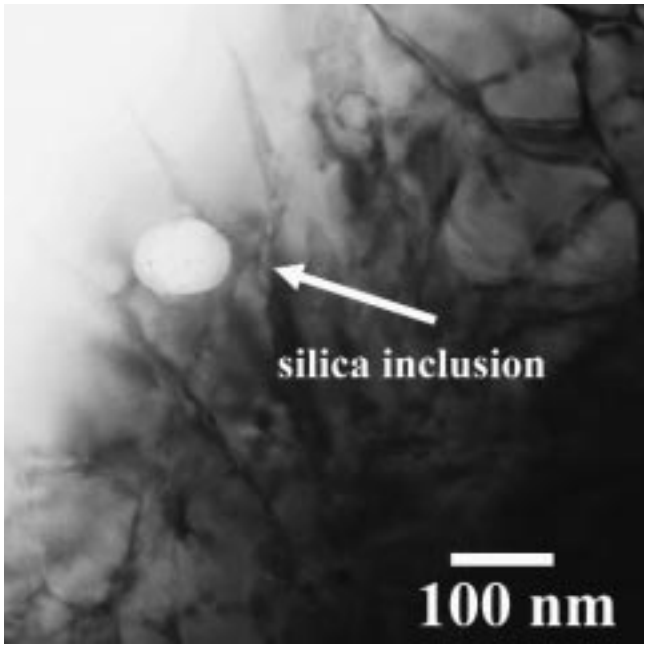

Fig. 5 TEM micrograph of the silica inclusion. Most silica inclusions were found interior to the splats with nearly spherical morphology having sizes ranging from hundreds of nanometers to a few microns in diameter.

Table 6 Comparative elemental results for samples annealed at 1800 °C for various times

At.%	2 h	6 h	10 h
Mo	53.9	55.4	56.7
Si	33.7	30.4	29.7
B	10.1	9.7	9.6
O	0.19	2.21	1.98
N	0.31	0.43	0.27
C	1.80	1.89	1.74

evaporative loss of Si. However, even in the nominally inert environment of the chamber, there was still substantial uptake of oxygen in the alloy, predominately in the form of silica. The as-sprayed microstructure was spatially inhomogeneous, reflecting the inhomogeneities in the feed stock. Yet, densities in excess of 90% theoretical can be achieved by thermal spraying. Recrystallization of the alloy occurs rapidly at 1800 °C with a small increase in density with longer annealing time. Silica is not removed by annealing. This is important since high silica content has a negative effect on the mechanical behavior at high temperatures due to viscous flow of the silica.[5]

Acknowledgments

The Ames Laboratory is operated by the U.S. Department of Energy (DOE) by Iowa State University under Contract No. W-7405-ENG-82. This work was supported by the Office of Energy Research, Office of Computational and Technology Research, Advanced Energy Projects Division.

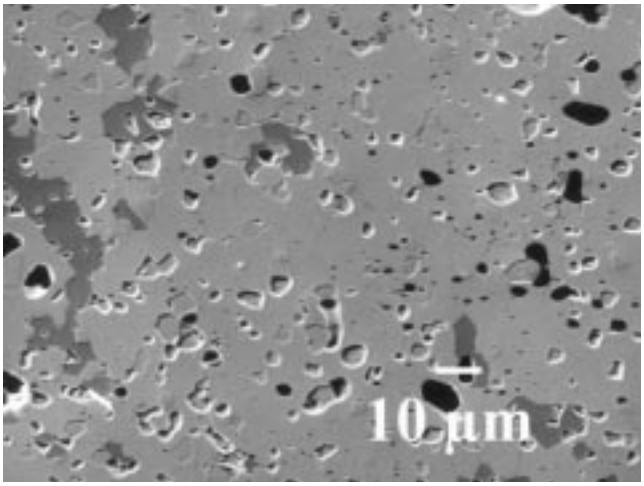

Fig. 6 SEM micrograph of the monolithic sample annealed at 1800 °C for 2 h. Note the complete recrystallization of the microstructure compared to the as-sprayed microstructure (Fig. 2). The uniformly light gray region is T1, the dark gray is $MoSi_2$, and the slightly recessed regions (due to Murakami's etching) are MoB. There is both porosity and silica. The silica is typically characterized by its uniformly black appearance and lack of rounding at the edges.

References

1. J.H. Schneibel, C.T. Liu, L. Heatherly, and M.J. Kramer: *Scripta Metall.*, 1998, vol. 38(7), pp. 1169-76.
2. A. Costa e Silva and M.J. Kaufman: *Intermetallics*, 1997, vol 5, pp. 1-15.
3. A.J. Thom, M.K. Meyer, Y. Kim, and M. Akinc: in *Processing and Fabrication of Advanced Materials for High Temperature Applications—III*, T.S. Srivatsan, and V.A. Ravi, eds., TMS, Warrandale, PA, 1994, pp. 413-37.
4. E.N. Ross and M.J. Kaufman: *22nd Conf. on Composites, Advances Ceramics and Structures*, D. Bray, ed., ACERS, Cocoa Beach, FL, 1998, pp. 421-28.
5. S.C. Okumus, Ö. Ünal, M.J. Kramer, and M. Akinc: in *Innovative Processing and Synthesis of Advanced Ceramics and Composites*, N.P. Bansal and J.P Singh, eds., *Ceram. Trans.*, 1999, vol. 94, pp. 347-60.
6. S. Sampath, R. Tiwari, and H. Herman: in *Microstructural Design by Solidification Processing*, E.J. Lavernia and M.N. Güngör, eds., TMS, Warrandale, PA, 1992, pp. 151-60.
7. F. Chu and D.J. Thoma: *22nd Conf. on Composites, Advances Ceramics and Structures*, D. Bray, ed., ACERS, Cocoa Beach, FL, 1998, pp. 413-20.
8. E. Kubel, Jr.: *Adv. Mater. Processing*, 1990, vol. 138, pp. 24-26.
9. D.J. Sordelet, M.J. Kramer, and Ö. Ünal: *J. Thermal Spray Technol.*, 1995, vol. 4, pp. 235-44.
10. S. Sampath, and H. Herman: *J. Met.*, 1993, vol. 45, pp. 42-49.
11. S. Sampath, and H. Herman: *J. Thermal Spray Technol.*, 1996, vol. 5, pp. 445-56.
12. R. Tiwari, H. Herman, and S. Sampath: *Mater. Sci. Eng.*, 1992, vol. A144, pp. 95-100.